TECHNICAL ARTICLE

Grain Refinement and Fading Behavior of MgB$_2$-Inoculated Magnesium

P. Emadi[1] · M. Rinaldi[1] · C. Ravindran[1]

Abstract

The light-weighting of automobiles is a prominent strategy toward increasing fuel efficiency, electric vehicle range and decreasing harmful emissions. As a light structural metal, magnesium has the potential to replace high density alloys such as steel. Based on lattice disregistry calculations, MgB$_2$ was identified as a potent inoculant for magnesium. In this research, permanent mold castings of pure Mg refined with MgB$_2$ were prepared and characterized using scanning electron and optical microscopy. Experimental results suggested that the primary Mg phase heterogeneously nucleated on the MgB$_2$ particle surfaces, leading to a 36% reduction in grain size relative to the unrefined condition. The effect of MgB$_2$ on grain refinement fading was also examined by preparing cast Mg samples refined with micro- and nano-particles of MgB$_2$, with melt holding periods of 5, 10 and 20 min. The results indicated that the micro-particles were susceptible to fading and that the holding time should not exceed 5 min. It was also determined that the castings refined with nano-particles were more resistant to fading. The results from this study indicated that MgB$_2$ displayed considerable potential as a grain refiner for Mg castings, with nano-particles especially suited to more complex commercial casting processes requiring longer melt holding times.

Keywords Casting and solidification · Magnesium · Electron microscopy · Optical microscopy · Metallography · Grain refinement

Introduction

The development of improved structural materials with greater strength-to-weight ratios has been one of the primary challenges in the automotive and aerospace industries. Lighter materials have the potential to improve fuel efficiency and to reduce harmful greenhouse gas emissions [1]. As a result, significant consideration is paid to light structural metals, such as magnesium (Mg), due to its low density, good machinability and abundance [2]. However, relatively low strength, poor ductility and creep resistance limit the effective use of Mg in industrial applications. Therefore, in order to promote the increased use of Mg in industry, its mechanical properties must be enhanced.

An effective method for improving the mechanical properties of Mg alloys is through grain refinement. Grain refinement can be achieved by the addition of inoculants that promote heterogeneous nucleation, which leads to the formation of more grains per unit volume [3]. This is desirable in cast Mg alloys, as it improves structural uniformity, reduces segregation and associated casting defects, and enhances consistency in performance. Several potential grain refiners and grain refining techniques have been identified and developed for Mg alloys. Some examples are melt superheating [4], the Elfinal process [5] and carbon inoculation [6]. However, these methods are currently inadequate, due to their many associated difficulties, including lengthy refining times, reductions in crucible life and increases in both fuel and electricity costs. Researchers have also experimented with titanium-, silicon-, and calcium-based refiners. However, addition of these compounds is often difficult, due to poor wetting or the formation of intermetallics that are detrimental to overall mechanical properties [7–15].

In order to achieve adequate refinement, grain refiners must be given sufficient melt interaction time (contact time) for the purpose of particle suspension and wettability. If inoculant particles remain in the melt past the appropriate contact time, their effectiveness is reduced through a

✉ P. Emadi
  payam.emadi@ryerson.ca

[1] Centre for Near-net-shape Processing of Materials, Ryerson University, 350 Victoria Street, Toronto, ON M5B 2K3, Canada

phenomenon known as fading. Limmaneechivitr and Eidhed [16], as well as Shaffer and Dahle [17], found that one of the sources of fading is the settling of grain refining particles at the bottom of the melt crucible. Moreover, grain refiner fading can also occur through refiner vaporization or oxidation, which is caused by high melt vapor pressure and high affinity for oxygen, respectively [18]. The former renders the additive ineffective due to the separation of the refiner from the melt, whereas the latter entails a reaction with oxygen to form a completely new compound, without the grain refining properties of its reactant [18].

The present work aims to investigate a unique, efficient and commercially viable grain refiner for Mg. Magnesium boride (MgB_2) meets the necessary requirements to act as an effective nucleating agent for Mg due to the following reasons. Similarity between the crystal structures of the host metal and the inoculant. Magnesium boride has an HCP crystal structure with lattice constants of $a = 0.307$ nm and $c = 0.352$ nm [19], whereas those of Mg are $a = 0.320$ nm and $c = 0.520$ nm [20]. Non-dissolution of the grain refining particles in the liquid host metal. As well, MgB_2 possesses many desirable properties, such as low density (2.57 g/cm^3 [19]), high melting temperature (830 °C [19]), and good thermal stability. However, information pertaining to the effective MgB_2 particle size range, fading behavior and interactions with the melt has not been previously pursued. Therefore, the current study examines the effects of reinforcing pure Mg with micro- and nano-sized particles of MgB_2 in an effort to elucidate its effects on grain refinement and fading.

This study was performed on pure Mg to remove the effects of various alloying elements on the response of molten Mg to inoculation, since alloying elements may alter the melt liquid properties, such as surface tension or viscosity. With the baseline data established in this study, the potential for the application of MgB_2 to Mg alloy systems will be investigated. This will aid in producing grain-refined lightweight alloys with improved resistance to fading.

Materials and Methods

Ball Milling and Particle Size Analysis

Planetary ball-milling was performed using a Retsch Planetary Ball Mill (model PM 100) to decrease the as-received MgB_2 particle size. Tungsten carbide (WC) milling media (3 mm in diameter) and a 50 mL WC-based grinding jar were used during the milling process. Approximately 60% of the jar volume was filled with grinding media to increase the friction surface required for producing fine particles. Next, 30% of the grinding jar volume was filled with sample material, and the remaining 10% was left empty. Since the target

particle size was in the nano-range, a colloidal grinding procedure using isopropyl alcohol with 99.99% purity as a dispersing agent was utilized. The MgB_2 powder was ball-milled for a total of 480 min at 300 rpm in 30 min intervals. Each milling interval consisted of three 10 min phases: (1) clockwise grinding, (2) cooling and (3) counter-clockwise grinding. Once the milling was complete, the powder was allowed 60 min to sufficiently cool before removal.

To analyze the change in particle size, four samples of the ball-milled powder were taken at 60, 240, 360 and 480 min of grinding time. Particles from the as-received powder were classified as micro-particles. Particles from powders ground for 480 min were classified as nano-particles. Particle size determination was performed by first stopping the ball-mill at the specified time and diluting a minor sample of MgB_2 powder in ethanol. The particles within the diluted sample were then evenly distributed throughout the solution using a Branson ultrasonic bath (model B-32) for 30 s. The solution was then dropped on a brass rod for observation using a JEOL scanning electron microscope (SEM) (model 6380LV) equipped with an energy-dispersive X-ray spectrometer (EDS) at a beam voltage of 20 keV. Using the SEM images, the area of each particle was measured with Buehler Omnimet image analysis software, and the effective diameter of each particle was calculated. With this analysis technique, the particle size distribution for each milling interval was determined.

Melting and Casting

Cast samples were prepared by preheating approximately 1 kg of commercial purity (99.9%) Mg ingots at 250 °C in an electric resistance furnace. Following this, the ingots were molten in the same electric resistance furnace at a temperature of 775 °C within a low-carbon steel crucible. A cover gas consisting of 4.7 L/min of CO_2 with 0.5 vol.% SF_6 as used to prevent oxidation. For each casting, the desired amount of MgB_2 powder was added to the melt and stirred at 300 rpm for 3 min using a low-carbon steel impeller. After 5 min of holding the melt in the furnace, a portion was poured into a graphite mold, preheated to 750 °C, at a pouring temperature of 720 °C. The resultant castings were cylindrical samples with a hemispherical bottom, 40 mm in diameter and 50 mm in height. Two subsequent castings were produced in similar graphite molds using the same batch of material after 10 and 20 min holding times. Table 1 presents a summary of casting parameters used in this study. The average chemical composition of the Mg ingots, measured using an Oxford Instruments Foundry-Master Pro optical emission spectrometer, is presented in Table 2. For each casting condition, two trials were prepared to ensure repeatability of the results.

Table 1 Summary of casting parameters for grain size and fading experiments

Pouring temperature, °C	Mold temperature, °C	Holding time, min	MgB₂ particle size range	MgB₂ addition level, wt.%
720	750	5, 10, 20	Micro	0.0125
				0.02
				0.025
				0.03
				0.05
				0.1
			Nano	0.025

Grain Size Analysis

Samples for grain size analysis were sectioned 20 mm from the bottom surface of the castings, along the diameter, and were ground using silicon-carbide papers with water as a coolant. Polishing was performed using 5, 3 and 1 μm alumina-ethanol suspensions. The samples were final polished with a 0.05 μm colloidal alumina and silica blend which also acted as an etchant. An ethanol rinse was used to stop the etching process and compressed air was used to dry the samples.

Grain size measurements were performed immediately after polishing, using macrographs captured over the entire sample surface. The images were taken using a Nikon D5300 digital camera equipped with an AF-S Micro NIKKOR lens with a 60 mm focal length and a maximum aperture of approximately 21.43 mm (*f*/2.8). The circular intercept procedure detailed in ASTM E112-13 [21] was used to measure grain size, since the grain morphology of the samples consisted of both columnar and equiaxed grains.

Results and Discussion

Lattice Disregistry Modeling

The grain size of an alloy is highly influenced by insoluble impurities in the liquid metal. Often, grain refinement will be facilitated by adding carefully selected impurities or particles for heterogenous nucleation. Considering the typical criteria used to select a nucleating particle, as explained previously, lattice similarity plays a key role. This is due to the interfacial strain energy between the grain refining particle substrate and the host liquid metal. In effect, due to the difference in lattice configuration between the solidifying liquid metal and grain refining substrates, an energy barrier for heterogeneous

nucleation is induced by the rearrangement of solidifying liquid atoms [22]. Further, the level of lattice matching between the particle and the matrix has been shown to have direct correlation with the level of interfacial energy or the energy barrier [23]. Closely matching lattices require less energy for the formation and growth of a crystal as compared to those with poor coherence. Thus, lattice coherence between the substrate and the matrix is an important factor for effective grain refinement through heterogenous nucleation.

In this study, the Bramfitt model [24] was used to predict the effectiveness of the inoculant as a potential grain refiner for Mg. The model, also known as the plane-to-plane matching model, uses crystallography as a basis to determine the nucleating potential for a particle and matrix system. This was done by comparing the interatomic spacing and the close-packed directions of pairs of low index close-packed planes between the nucleating particles and the host metal. The Bramfitt model can be expressed by Eq 1.

$$\delta_{(hkl)_n}^{(hkl)_s} = \frac{\sum_{i=1}^{3} \frac{\left| d_{[uvw]_s^i} \cos\theta - d_{[uvw]_n^i} \right|}{d_{[uvw]_n^i}}}{3} * 100 \qquad (1)$$

where *n* and *s* denote the nucleus/matrix and the inoculant/substrate, respectively, (*hkl*) is a low-index close-packed plane, [*uvw*] is a low-index direction on the (*hkl*) plane, and *θ* is the angle between a pair of adjacent low-index directions on the (*hkl*) plane.

In order to determine an effective inoculant for Mg, compounds were evaluated with regard to their crystallographic matching with the host matrix. Following this assessment, MgB₂ was identified as a potential refiner for Mg grains, as described herein. The low-index close-packed planes for Mg and MgB₂ were determined to be the (0001) planes, which are shown in Fig. 1. To illustrate the resemblance of their crystal structures, the figure displays a geometrically scaled version of the (0001) planes of Mg and MgB₂ superimposed on each other. The figure elucidates the high level of similarity between the two crystal structures, and thus, it is likely that MgB₂ can act as an efficient grain refiner for Mg.

The planar disregistry value calculated for the Mg-MgB₂ system is presented in Table 3. The minimum disregistry for the system was calculated to be 4.36%. According to Bramfitt, this value falls within the highly effective range (< 6%), which suggests that the Mg phase will nucleate on MgB₂ particles based on their orientation relationship [24]. Several other orientations were also examined, such as (0001)‖(10$\bar{1}$0) and (10$\bar{1}$0)‖(10$\bar{1}$0), but they did not fall within the required disregistry

Table 2 Average chemical composition of the pure Mg ingots (wt.%)

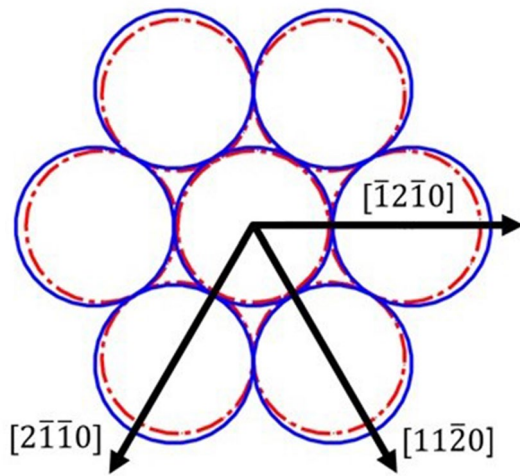| Mg	Zn	Zr	Mn	Fe	Si	Ni	Al	Cu	Others
99.9	0.0013	0.0051	0.011	0.016	0.0058	0.0051	< 0.0030	< 0.0020	< 0.025

Fig. 1 Superposition of basal planes for Mg (blue-solid) and MgB$_2$ (red-dashed)

range. Thus, based on these calculations, an experimental investigation was warranted to validate the effectiveness of MgB$_2$ as a grain refiner for Mg and its alloys.

Preparation of Inoculants

The particle size distribution of the as-received MgB$_2$ powder, measured using SEM images, can be seen in Fig. 3. The distribution indicated that the as-received particles, hereafter referred to as micro-particles, were approximately 0.8 µm in size.

Figure 2 compares the micro-MgB$_2$ particles (Fig. 2a) with the particles subjected to 480 min of ball-milling (Fig. 2b). The figures indicate that the ball-milling procedure significantly reduced the average particle size. The reduction in particle size occurred as a result of ruptured interatomic bonds, leading to the cleavage fracture of crystalline grains and the formation of new surfaces [25].

The measured particle size distributions for the ball-milled samples can be seen in Fig. 3. The results show that after 60 min of milling, the average particle size decreased from 0.8 to 0.5 µm. With increasing milling time to 240 and 360 min, the particle size further decreased to 0.3 and 0.2 µm, respectively. At 480 min of milling, the MgB$_2$ particles had been successfully reduced to an average diameter of 100 nm. Particles milled for 480 min will hereafter referred to as nano-particles.

Figure 4 shows the MgB$_2$ particle size distribution as a function of ball-milling time. As described previously, with increasing milling time, the particle size decreased. However, it can be observed that after the 60 min, the rate of particle size reduction with further milling time is reduced. This observation can be explained by a study performed by Gusev and Kurlov [26], which reported a gradual decrease in the particle size up to a saturation value. The researchers suggested that saturation occurs due to the buildup of microstrains after the initial stages

Table 3 Calculated values of planar disregistry between Mg and MgB$_2$ for (0001) planes

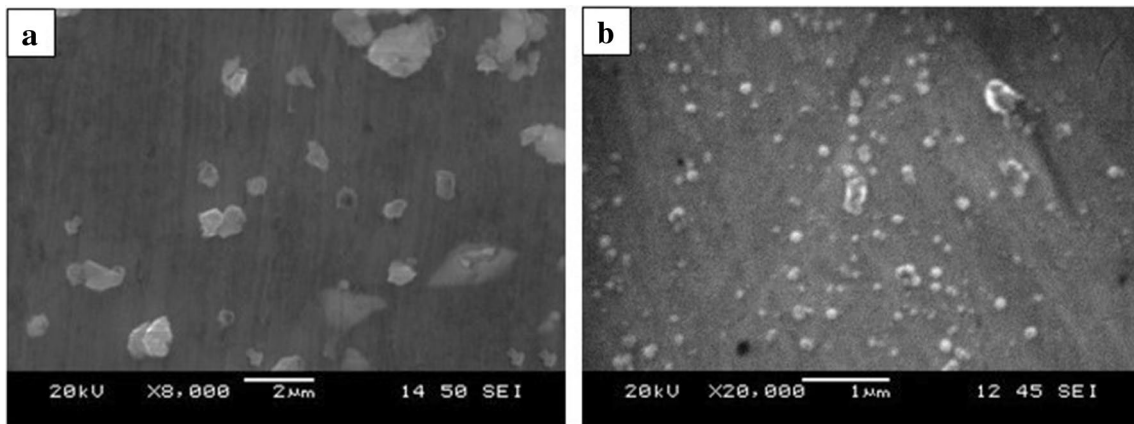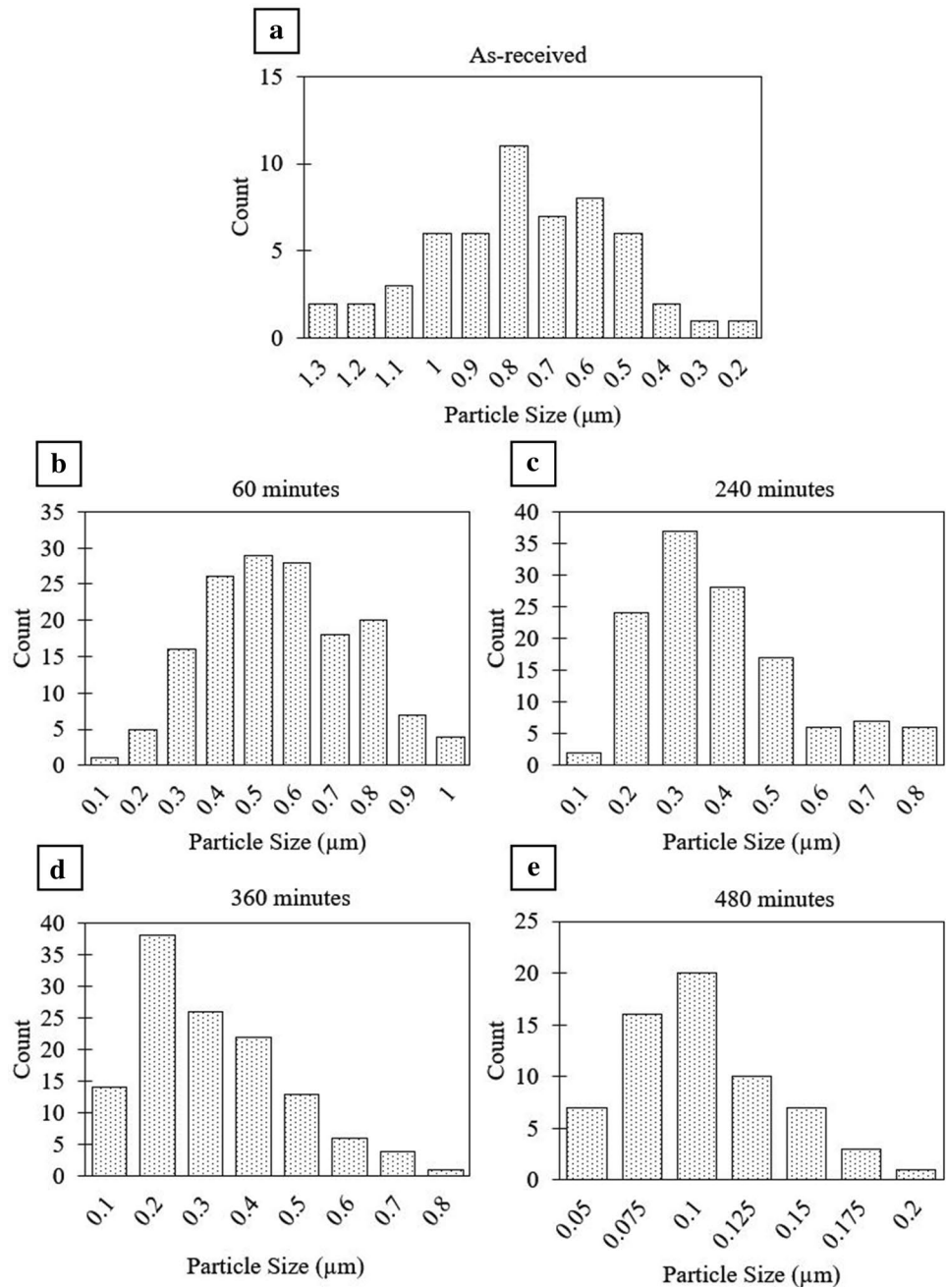|	$[uvw]_s$	$[uvw]_{Mg}$	$d[uvw]_s$, nm	$d[uvw]_{Mg}$, nm	θ, °	$d[uvw]_s * \cos(\theta)$, nm	$\delta^{(hkl)_s}_{(hkl)_{Mg}}$
$(0001)_{MgB2} \parallel (0001)_{Mg}$	$2\,\overline{1}\,\overline{1}\,0$	$2\,\overline{1}\,\overline{1}\,0$	0.307	0.321	0	0.307	4.36%
	$11\,\overline{2}\,0$	$11\,\overline{2}\,0$	0.307	0.321	0	0.307	
	$\overline{1}\,2\,\overline{1}\,0$	$\overline{1}\,2\,\overline{1}\,0$	0.307	0.321	0	0.307	

Fig. 2 SEM images of the MgB$_2$ particles (**a**) as-received and (**b**) after 480 min of ball milling

Fig. 3 MgB$_2$ particle size distributions after ball milling for (**a**) as-received, (**b**) 60 min, (**c**) 240 min, (**d**) 360 min and (**e**) 480 min

of the milling process, which can impede further particle size reductions.

Microstructural Analysis and Effect of MgB$_2$ Micro-Particle Addition Level

This section summarizes the effect of the as-received (micro-sized) MgB$_2$ particle addition on the grain size of Mg. An optical macrograph of the pure Mg sample is shown in Fig. 5a. The average grain size for the unrefined condition was 2470 μm (Fig. 9). The microstructure consisted of an

ingot type structure, featuring columnar grains along the periphery and equiaxed grains in the center of the casting.

The average grain sizes of the samples refined with varying levels of MgB$_2$ are presented in Fig. 9. When 0.0125 wt.% MgB$_2$ was added, the average grain size reduced from 2470 to 1940 μm. Further increases in MgB$_2$ addition to 0.02 wt.% led to an additional reduction in grain size to 1730 μm. The most effective grain refinement of Mg was achieved with the 0.025 wt.% addition level, which produced an average grain size of 1580 μm (Fig. 5b). The grain structure of this casting was 36% finer than that of the
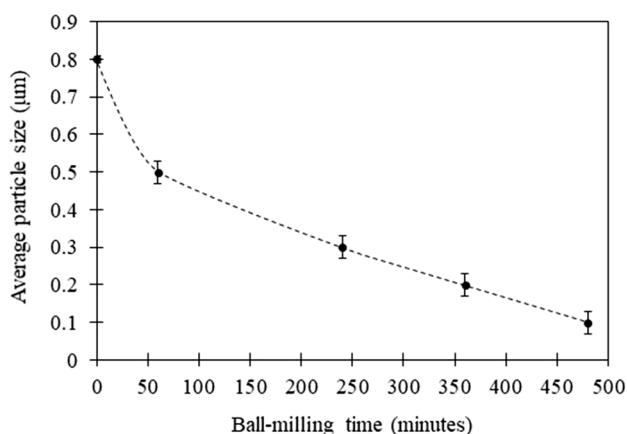
Fig. 4 Variation of average particle size as a function of ball-milling time with error bars equaling $\pm \sigma$

base casting. However, with greater additions of MgB_2 in the range of 0.03-0.1 wt.%, no further refinement was seen. By performing an analysis of variance, the changes in grain size between the unrefined samples and the samples with 0.02 wt.% MgB_2 were determined to be statistically significant, whereas changes from 0.02 to 0.1 wt.% were determined to be insignificant.

Considering the low lattice disregistry (4.36%), it was thought that the refinement resulted from MgB_2 particles acting as heterogeneous nucleation sites during solidification. Furthermore, it was observed that the grain boundary shape changed from smooth and laminar in the base metal to serrated for the well-modified samples (Fig. 5). This may be a result of the rejection of MgB_2 particles toward the grain boundaries during solidification.

As mentioned above, insignificant change in grain size was observed at addition levels greater than 0.02 wt.% MgB_2, which suggests that the nucleants became saturated

in number. This typically occurs since the increased number of nucleants results in a higher frequency of particle-to-particle collisions. As a result, the particles coalesce, agglomerate and settle at a faster rate, which decreases the total number of available nucleating substrates [27]. Consequently, the refinement achieved for MgB_2 levels at and above 0.025 wt.% remained comparable to the 0.02 wt.% condition. Since they are still significantly refined relative to the base Mg casting, 0.025 wt.% additions are recommended for reaching the finest possible grain size, as the extra addition would ensure that the amount of MgB_2 added falls in a range near 0.02 wt.% (and not significantly less). These finding are of high importance in a commercial setting, since: (1) a relatively minor quantity of grain refiner can lead to significant refinement, and (2) a wide addition range between 0.0125 and 0.1 wt.% could be implemented while still achieving suitable results. This is significant, since typical industrial-scale measurements are not as precise as measurements taken in a laboratory setting.

Microstructure examination using SEM was performed on the base Mg and grain-refined castings. Samples were examined in the same area that was used for the grain size measurements to identify the particles responsible for grain refinement and to observe whether any reactions occurred within the melt. The samples with higher amounts of MgB_2 were used, since boron is a light element and its detection in small quantities using SEM is difficult. Evidence of MgB_2 in the alloy was found in the Mg + 0.1 wt.% MgB_2 castings in two main locations: within the grains and along the grain boundaries. Figure 6a shows an MgB_2 agglomerate within an α-Mg grain. Using EDS, it was found to consist primarily of Mg, O, and B (Fig. 6b). This indicated that the particle was likely MgB_2, as expected. This observation confirmed the presence of MgB_2 in the liquid metal, and it followed that the particles may have aided in the refinement of α-Mg grains by increasing the number of nucleation sites. These results are

Fig. 5 Macrographs of etched (**a**) pure Mg and (**b**) Mg refined with 0.025 wt.% micro-MgB_2
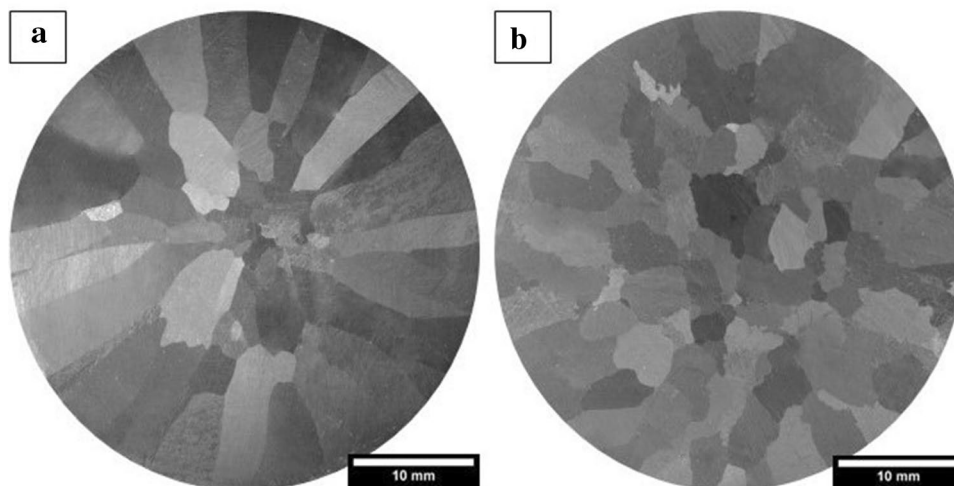
similar to a study performed by Suresh et al. [28], in which boron-based particles were observed within the centers of grains and acted as nucleating sites.

Figure 7 displays a similar MgB_2 agglomeration of particles found along a grain boundary. This indicated that the finer grain size in the MgB_2 refined samples may also be attributed to particle/solidification front interactions, which is the subject of several investigations [29, 30]. When a moving solid--liquid interface (solidification front) approaches a suspended foreign particle, the particle can be either pushed away from it or captured. It follows that the interactions can result in a reduced growth rate for the primary Mg phase, since the presence of MgB_2 particles on the edges of the Mg grains likely create diffusion barriers to growth [31–33]. Moreover, this may be the reason for the serrated type of grain boundaries observed in the microstructure.

Despite the low lattice disregistry between MgB_2 and Mg for the $(1000)_{MgB2}//(1000)_{Mg}$ orientation relationship, all other orientation relationships were determined to be unsuitable for effective heterogeneous nucleation ("Lattice Disregistry Modeling" section). This suggested that effective heterogeneous nucleation only occurs when the (0001) basal planes of MgB_2 particles are exposed to the melt, and Mg nuclei form with a basal plane in contact with the particle surface. The remaining particles without this favorable orientation relationship would likely be pushed away by the solidification front. This is in agreement with the observation that only some of the MgB_2 particles are able to nucleate the primary Mg phase in the refined castings, while others are pushed toward the grain boundaries.

Grain Refiner Fading Analysis

The microstructural changes with increases in grain refiner holding time are shown in Fig. 8. For the micro-particle refined castings, the increased holding time resulted in an appreciable growth in average grain size. Figure 9 displays the average grain sizes at 5, 10 and 20 min of holding
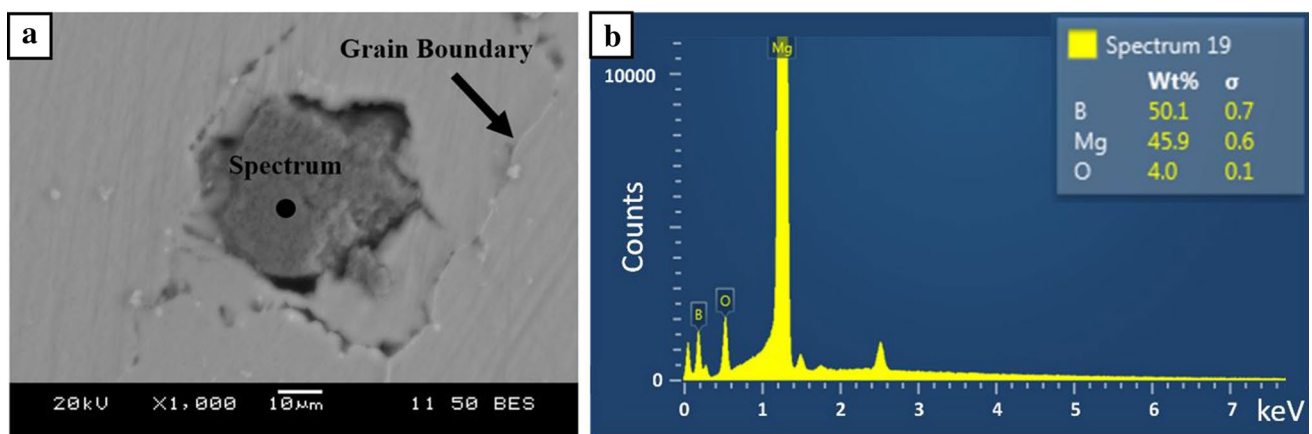

Fig. 6 MgB_2 agglomerate (**a**) SEM image and (**b**) EDS point spectrum analysis
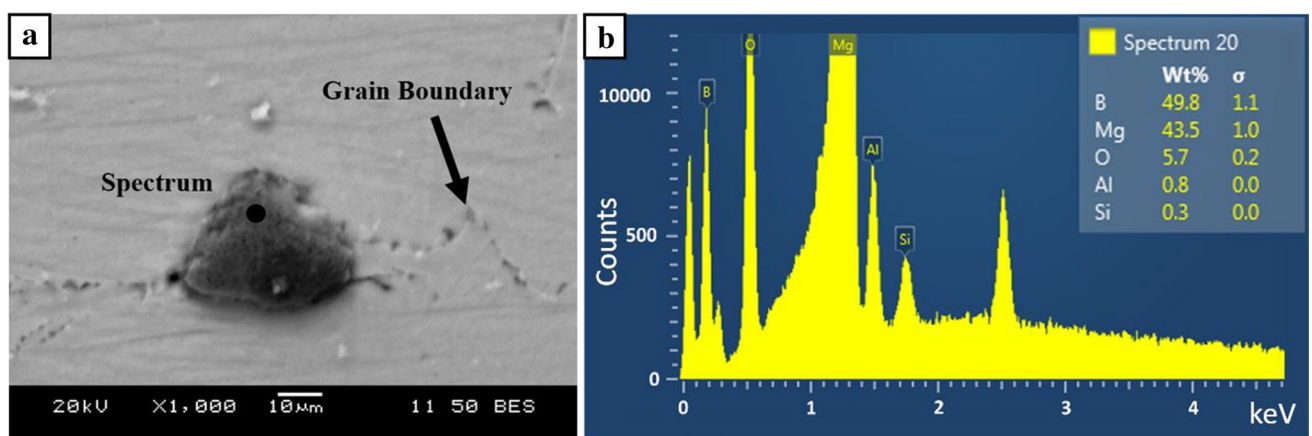

Fig. 7 Second MgB_2 agglomerate (**a**) SEM image and (**b**) EDS point spectrum analysis

following addition. At the initial holding time of 5 min, there was a significant improvement in grain size. However, with longer holding times, the refining effects were reduced, leading to effectively no difference at 20 min with any addition level below approximately 0.02 wt.% and above 0.05 wt.%. As mentioned in the previous section, the most effective grain refinement of Mg was achieved at the 0.025 wt.% addition level with 5 min of holding. This led to an average grain size of 1580 μm. At 10 min of holding with 0.025 wt.% addition, the grain size increased to 1940 μm. At the 20 min holding time interval, the grain size increased to 2080 μm. Consequently, at 20 min of holding, the effectiveness of MgB_2 as a grain refiner was reduced by nearly 32%.

Grain refinement fading is a common phenomenon in cast alloys [34]. In this study, fading effects were consistently observed. These effects were attributed to particle settling, which is a result of the difference in density of Mg (1.74 g/cm^3 [20]) and MgB_2 (2.57 g/cm^3 [19]) [35]. As the holding time increased, the denser MgB_2 particles may have settled to the bottom of the crucible, thereby reducing the number of potent nucleants within each casting [34]. Moreover, for each casting, liquid metal was ladled from the top of the crucible, which could have further contributed to the fading effects.
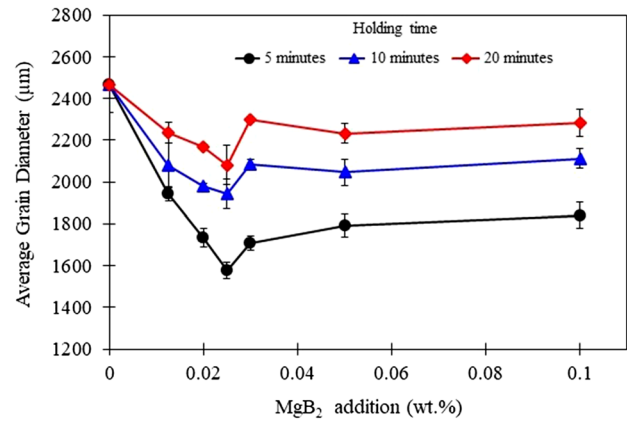
Fig. 9 Effect of MgB_2 micro-particle addition level and holding time on the grain size of Mg (error bars represent twice the standard deviation on the sample mean, $\pm\,\sigma$)

In efforts to improve upon the trends found with the micro-particles, castings were performed using nano-particles at 0.025 wt.%. This addition level was chosen since it provided the largest degree of refinement. Figure 8 shows macrographs of grain sizes comparing both micro-particle and nano-particle inoculated castings over a range of holding
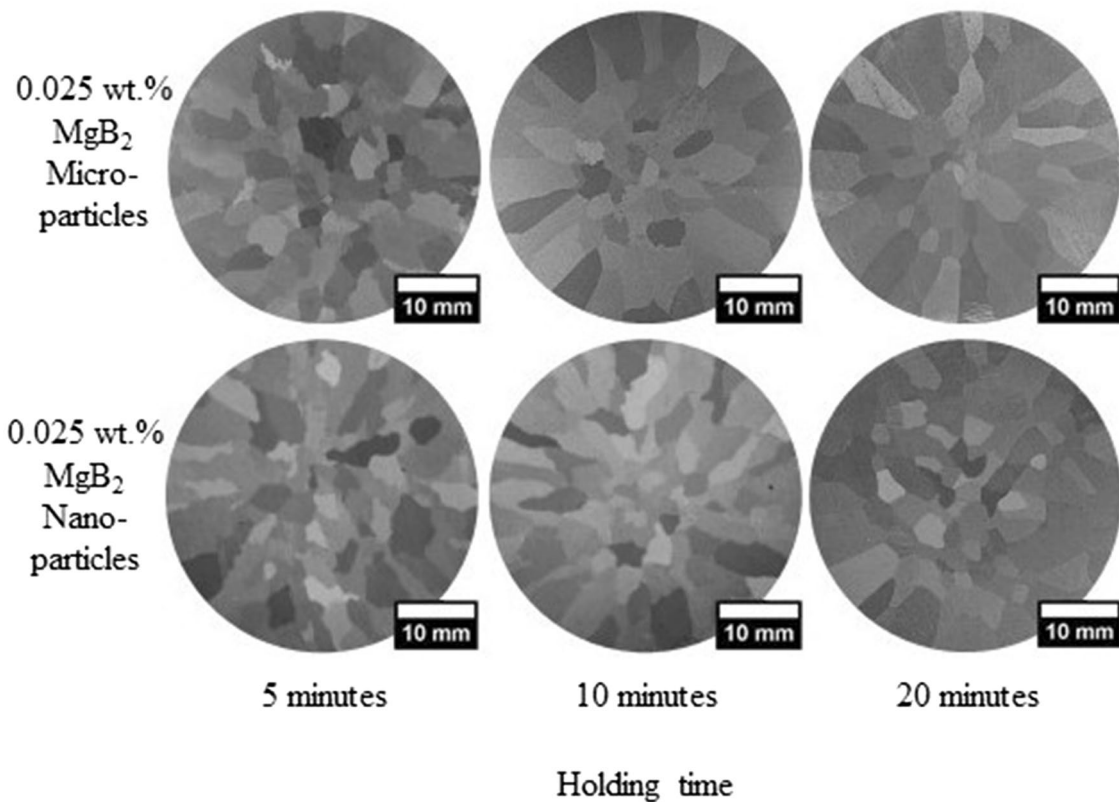
Fig. 8 Optical macrographs showing grain structures of Mg refined with MgB_2 micro- and nano-particles, with 5, 10, and 20 min of holding time
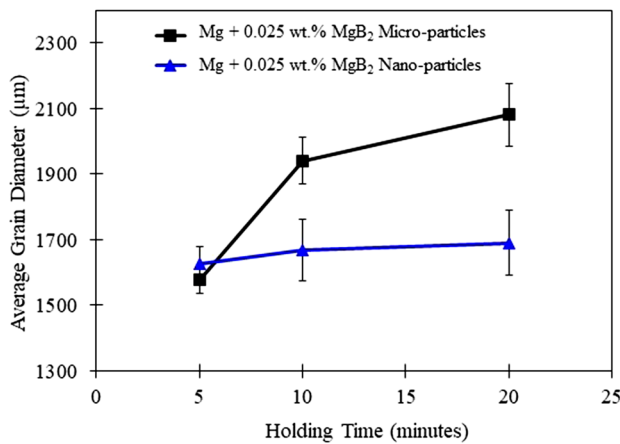
Fig. 10 Effect of MgB_2 particle size and holding time on the grain size of Mg at 0.025 wt.% addition (error bars represent twice the standard deviation on the sample mean, $\pm\,\sigma$)

times. Visually, it was noticed that the nano-particles refined more effectively at longer holding times. Quantitatively, it was found that the castings refined with nano-size MgB_2 particles displayed a significant resistance to fading within the 20 min time interval. Figure 10 compares the effectiveness of MgB_2 micro-particles and nano-particles on the grain size of Mg at 5, 10 and 20 min of holding time. The grain size of castings refined with 0.025 wt.% nano-particle MgB_2 at 5 min holding time was 1630 μm (34% reduction compared to the base casting), which were comparable to the 0.025 wt.% micro-particle refined castings (1580 μm). At 10 min of holding, the grain size only increased to 1670 μm, and at 20 min of holding, the grain size increased to 1690 μm. Thus, considering the error bars, it can be concluded that the grain sizes of the castings refined with nano-MgB_2 remained effectively unchanged within the 20 min holding period.

Figure 10 clearly displays that the castings refined with nano-particles were more resistant to fading than those refined with micro-particles. This occurrence can be explained by Stokes' law [17], which states that the settling behavior of particles is subject to the particle size, characteristics, and density. The size of the grain refiner particles can impact the settling rate, and Stokes' law predicts that larger grain refiner particles settle at a faster rate than smaller particles. Following this, the grain size of the nano-particle refined castings likely remained stable throughout the 20 min holding time.

The wide range of effectiveness for nano-particle MgB_2 is of high importance, especially in an industrial setting where holding times are typically not as exact as in laboratory settings, and the furnace-to-mold distance can be much larger. In addition, the varying resistance to fading allows the refiner to be tailored to the casting process as well as to other grain refiners and their alloying additions. One such example

is manganese, which is a common alloying element for Mg that requires long holding times because of its limited solubility. Therefore, it is recommended that the micro-particle inoculant can be used successfully only in the continuous casting or in-mold grain refinement where there is less time lost in casting procedures.

In summary, both micro- and nano-sized MgB_2 particle additions to Mg effectively reduced the average grain size. Moreover, the castings refined with nano-particles were determined to be highly resistant to fading effects. These results indicated that MgB_2 has much potential as a grain refiner, and its application to commercial Mg alloys warrants investigation. Doing so may promote their increased use in the automotive and aerospace industries.

Conclusion

In this study, MgB_2 was proposed as a potent nucleant for the refinement of Mg. Particles were ball-milled for 60, 240, 360 and 480 min to reduce the average particle to 100 nm. Experimentally, the effectiveness of grain refinement and fading behavior of micro- and nano-sized particles of MgB_2 was investigated. Pure Mg samples were refined with MgB_2 micro-particle additions ranging from 0.0125 to 0.1 wt.%, as well as 0.025 wt.% nano-particle additions. The grain sizes of the castings were evaluated with 5, 10 and 20 min holding times following refiner addition. Based on lattice disregistry calculations and grain size analysis, it was found that MgB_2 was able to successfully refine Mg grains. The disregistry of 4.36% between Mg and MgB_2 led to a maximum refinement of 36% at 0.025 wt.% refiner addition, with suitable refinement achieved using 0.02–0.1 wt.% additions as well. It was suggested that refinement with MgB_2 occurred via both enhanced nucleation and grain growth restriction, indicated by the observation of MgB_2 particles at both grain centers and grain boundaries.

The sensitivity of the micro-particles to inoculation fading was relatively high. To obtain the most effective refinement with these particles, the holding time between addition and casting should not exceed 5 min. In contrast, the nano-particles were much more resistant to fading, due to their fine particle size, enabling much wider application to various casting systems. Further study of MgB_2 is warranted to determine its suitability as a grain refiner for cast industrial Mg alloys.

References

1. S. Kollamthodi, D. Kay, I. Skinner, C. Dun, S. Hausberger, *The Potential for Mass Reduction of Passenger Cars and Light Commercial Vehicles in Relation to Future CO2 Regulatory Requirements* (Ricardo-AEA, Harwell, 2015)
2. A. Luo, Recent magnesium alloy development for elevated temperature applications. Int. Mater. Rev. **49**, 13–30 (2004)
3. B. Shia, R. Chena, W. Kea, Influence of grain size on the tensile ductility and deformation modes of rolled Mg-1.02 wt.% Zn alloy. J. Magnes. Alloys. **1**, 210–216 (2013)
4. I. Polmear, Magnesium alloys and applications. Mater. Sci. Technol. **10**, 1–16 (1994)
5. E. Emley, *Principles of Magnesium Technology* (Pergamon Press, Oxford, 1966)
6. C. Li, S. Yang, G. Luo, H. Liao, J. Du, Revealing the nuclei formation in carbon-inoculated Mg-3%Al alloys containing trace Fe. Materials. (2019). https://doi.org/10.3390/ma12152478
7. K. Nie, Y. Guo, P. Munroe, K. Deng, X. Kang, Microstructure and tensile properties of magnesium matrix nanocomposite reinforced by high mass fraction of nano-sized particles including TiC and MgZn$_2$. J. Alloys Compd. **819**, 153348 (2020)
8. A. Elsayed, C. Ravindran, B. Murty, Effect of aluminum–titanium–boron based grain refiners on AZ91E magnesium alloy grain size and microstructure. Int. J. Metalcast. **5**, 29–41 (2011)
9. H. Tsukamoto, Enhancement of mechanical properties of SiCw/SiCp-reinforced magnesium composites fabricated by spark plasma sintering. Results Mater. **9**, 100167 (2021)
10. X. Ai, G. Quan, Effect of Ti on the mechanical properties and corrosion of cast AZ91 magnesium alloy. Open Mater. Sci. J. **6**, 6–13 (2012)
11. S. Ganguly, S. Sarkar, A.K. Mondal, Enhancement of tensile properties of AZ91–Ca–Sb magnesium alloy with SiC Nanoparticles Additions. Met. Mater. Int. (2020). https://doi.org/10.1007/s12540-020-00744-3
12. S. Liu, B. Li, X. Wang, W. Su, H. Han, Refinement effect of cerium, calcium and strontium in AZ91 magnesium alloy. J. Mater. Process. Technol. **209**, 3999–4004 (2009)
13. P. Xiao, Y. Gao, F. Xu, S. Yang, B. Li, Y. Li, Z. Huang, Q. Zheng, An investigation on grain refinement mechanism of TiB2 particulate reinforced AZ91 composites and its effect on mechanical properties. J. Alloys Compd. **780**, 237–244 (2019)
14. T. Davis, L. Bichler, F. D'Elia, N. Hort, Effect of TiBor on the grain refinement and hot tearing susceptibility of AZ91D magnesium alloy. J. Alloys Compd. **759**, 70–79 (2018)
15. Z.R. Zeng, Y.M. Zhu, J.F. Nie, S.W. Xu, C.H.J. Davies, N. Birbilis, Effects of Calcium on strength and microstructural evolution of extruded alloys based on Mg–3Al–1Zn–0.3Mn. Metall. Mater. Trans. A. **50**, 4344–4363 (2019)
16. C. Limmaneevichitr, W. Eidhed, Fading mechanism of grain refinement of aluminum–silicon alloy with Al–Ti–B grain refiners. Mater. Sci. Eng. A. **349**, 197–206 (2003)
17. P. Schaffer, K. Dahle, Settling behaviour of different grain refiners in aluminium. Mater. Sci. Eng. A. **413**, 373–378 (2005)
18. S. Hegde, K.N. Prabhu, Modification of eutectic silicon in Al–Si alloys. J. Mater. Sci. **43**, 3009–3027 (2008)
19. J. Jorgensen, D. Hinks, S. Short, Lattice properties of MgB$_2$ versus temperature and pressure. Phys. Rev. B. (2001). https://doi.org/10.1103/PhysRevB.63.224522
20. M. Avedesian, H. Baker, *Magnesium and Magnesium Alloys* (ASM International, Materials Park, 1999)
21. Standard Test Methods for Determining Average Grain Size. ASTM E112-13, ASTM (2013)
22. L. Wang, L. Yang, D. Zhang, M. Xia, Y. Wang, J. Li, The role of lattice misfit on heterogeneous nucleation of pure aluminum. Metall. Mater. Trans. A. **47A**, 5012–5022 (2016)
23. D. Turnbull, B. Vonnegut, Nucleation catalysis. Industrial engineering. Chemistry. **44**, 1292–1298 (1952)
24. B.L. Bramfitt, The effect of carbide and nitride additions on the heterogeneous nucleation behaviour of liquid iron. Metall. Trans. **1**, 1987–1995 (1970)
25. P. Butyagin, Mechanical disordering and reactivity of solids. Chem. Rev. **23**, 91–165 (1998)
26. A.I. Gusev, A.S. Kurlov, Production of nanocrystalline powders by high-energy ball milling: model and experiment. Nanotechnology. (2008). https://doi.org/10.1088/0957-4484/19/26/265302
27. C. Ti-jun, W. Rui-quan, H. Hai-jun, M. Ying, H. Yuan, Grain refining technique of AM60B magnesium alloy by MgCO3. Trans. Nonferrous Met. Soc. China. **22**, 1533–1539 (2012)
28. M. Suresh, A. Srinivasan, K. Ravi, U. Pillai, B. Pai, Influence of boron addition on the grain refinement and mechanical properties of AZ91 Mg alloy. Mater. Sci. Eng. A. **525**, 201–210 (2009)
29. J. Xu, L. Chen, H. Choi, X. Li, Theoretical study and pathways for nanoparticle capture during solidification of metal melt. J. Phys.: Condens. Matter. **25**, 539–543 (2012)
30. G. Lei, L. Song-Mao, C. Rong-shi, H. En-hou, Correlation of recalescence with grain refinement of magnesium alloys. Trans. Nonferrous Met. Soc. China. **18**, 288–291 (2008)
31. K. Nie, X. Wang, X. Hu, L. Xu, K. Wu, M. Zheng, Microstructure and mechanical properties of SiC nanoparticles reinforced magnesium matrix composites fabricated by ultrasonic vibration. Mater. Sci. Eng. A. **528**, 5278–5282 (2011)
32. K. Deng, K. Wu, X. Wang, Y. Wu, X. Hu, M. Zheng, W. Gan, H. Brokmeier, Microstructure evolution and mechanical properties of a particulate reinforced magnesium matrix composites forged at elevated temperatures. Mater. Sci. Eng. A. **527**, 1630–1635 (2010)
33. K. Deng, K. Wu, Y. Wu, K. Nie, M. Zheng, Effect of submicron size SiC particulates on microstructure and mechanical properties of AZ91 magnesium matrix composites. J. Alloys Compd. **504**, 542–547 (2010)
34. L. Lua, A. Dahle, Effects of combined additions of Sr and AlTiB grain refiners in hypoeutectic Al–Si foundry alloys. Mater. Sci. Eng. A. **435**, 288–296 (2006)
35. P. Mohanty, J. Gruzleski, Mechanism of grain refinement in aluminium. Acta Metall. Mater. **43**, 2001–2012 (1995)